

# Fundamental Investigation of Short-Range Inductive Coupling Wireless Power Transmission by Using Series-Series Capacitive Compensation Topology

Deeb Alashgar<sup>1</sup>, Koji Fujiwara<sup>2</sup>, and Naoto Nagaoka<sup>3</sup>

<sup>1</sup> Department of Electronic & Electrical Engineering, Doshisha University, cyjb3301@mail4.doshisha.ac.jp

<sup>2</sup> Department of Electronic & Electrical Engineering, Doshisha University, koji.fujiwara@mail.doshisha.ac.jp

<sup>3</sup> Department of Electronic & Electrical Engineering, Doshisha University, nnagaoka@mail.doshisha.ac.jp

## Abstract

*A Wireless Power Transfer (WPT) Systems was developed applying the concept of resonance theory. This paper is dedicated to a theoretical study of the series-series capacitive compensation topology, then devoted to the experimental implementation of this study to prove its validity. The experiments are set up to operate in 10-20 kHz frequency ranges at distances of 50 mm by using windings made of Litz wires to test the analytical design consideration. The results showed that the system's efficiency increased until reaching its peak at 80 % with a resonance of 20 kHz. The efficiency increases in accordance with resonance frequency. Although the theoretically calculated efficiency with an ideal transformer is 90.1 %, the actual efficiency obtained from the experiments in the laboratory at a coil distance of 50 mm and with a resonance frequency matching at 20 kHz is 80 %.*

## Keywords

*wireless power transfer systems, resonance theory, series-series capacitive compensation topology SS-CCT, size of the receiver's winding, efficiency*

## 1. INTRODUCTION

The method of wirelessly transferring electricity from power sources to the loads are currently gaining more attention from researchers in the field of power transmission for its geometric, economic and environmental advantages such as safety, and ease of maintenance. The technique of Wireless Power Transfer (WPT) System is defined as the transmission of electric energy from a power source into one or more electrical circuits or devices via magnetic induction or electric field through the air. WPT systems are classified into several types based on different factors such as the distance between the power source and load, which plays a significant role in determining which optimal system would achieve the required power transfer and desired efficiency, and affects the electromagnetic field and its characteristics. The magnetic field or the electric field will propagate to achieve power transmission in the near-field techniques. The field used in the system will determine which type of wireless power transmission should be implemented to transfer power within the region. The magnetic field is therefore used to transmit power in the inductive systems which also is called Inductive Wireless Power Transfer (IWPT) Systems, while the electric field is used to transmit power in the capacitive Wireless Power Transfer (CWPT) systems. CWPT system is

a method that has been recently proposed to transmit power from the source to the load wirelessly [Huang et al., 2014]. This system utilizes electric fields instead of magnetic fields to transfer power among the power source and the other loads. In IWPT systems, the inductive coupling occurs between two Coreless coils of wires as in [Choi et al., 2018] and it can be increased by putting a magnetic core of a ferromagnetic material, magnetic shields [Bibirica et al., 2017], or ferrite in the coils to raise the magnetic flux transferred from the transmitting coil to the receiving one. In the Short-Range Inductive Coupling (IC), the magnetic field is generated by the primary coil of the wireless power transfer system which propagates and radiates in all directions in the area surrounding it, but the distance between the two coils should be as short as possible to couple the most of the magnetic flux. The principle of mutual induction between the transmitting and receiving coils can be used to transfer the power wirelessly. In this paper, the IWPT system is investigated due to its advantages and facilities that match the demands of the electric system as shown in [Hassan and Elzawawi, 2015]. IWPT system transfers power from the primary to the secondary coil through a magnetic field, with different types of planar geometry being used to implement it, be them circular or rectangular. Yet notwithstanding the fact that rectangular geometry shows better tolerance to misalignment between the primary and secondary windings of the IWPT transformer [Boeij et al., 2006; Chopra, 2011]. This research focuses on circular geometry because of its preference coupling [Fernández et al., 2002] to improve the ef-

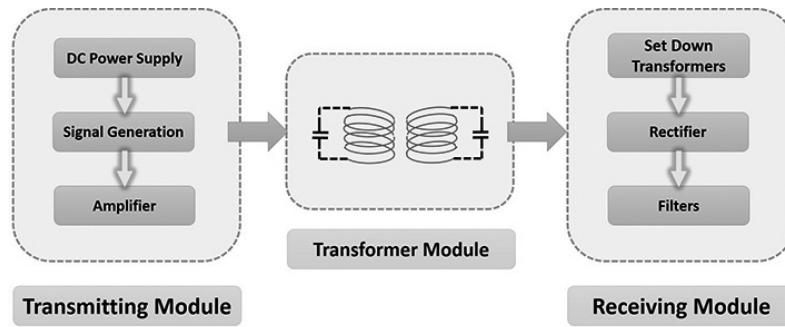


Fig. 1 Wireless power transfer (WPT) system

efficiency and hold the optimum distance of the capacitive compensated IWPT system.

## 2. THEORETICAL ANALYSIS

The basic IWPT system is introduced with a detailed physical and mathematical explanation. IWPT system is composed of three modules interacting with each other to perform a final function of the system as presented in Figure 3.

In this research, the transformer module (the windings) is discussed. The basic function of the transformer module is the transmission of the magnetic field. It has a plain structure made up of two windings separated by an air gap through which the power transfer occurs. The two windings are called the transformer module. Figure 2 illustrates the transforming windings with their compensation, and which are combined to form the transforming module.

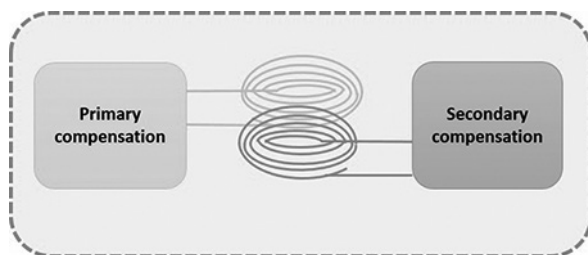


Fig. 2 The transformer module with its compensation

The principle of the resonance is used to achieve efficient power transfer through the air gap between the separated windings which are connected with capacitive compensators for reactive power. For this purpose, a number of structures of transformer windings have been proposed in many papers. The majority of these structures implemented a flat spiral shape [Shen et al., 2014; Ramezani et al., 2016], with only a few ones applying a non-flat spiral shape [Honjo et al., 2016]. At another level, most of these structures contain an air gap separating the two windings, while very few others use a magnetic core. Choosing the

most convenient shape of the transforming module is defined with a number of factors such as the air gap between the separated windings; harmonic effects; Skin depth losses; eddy current losses; size limitation; displacement insensitivity; weight of the magnetic core; and sensitivity to the misalignment between the separated windings. In this transforming structure, the air gap is taken into consideration because of its influence on the leakage inductance and mutual coupling, since a large air gap causes a large leakage inductance and a low mutual coupling, which in consequence implies a large magnetizing current. The SS-CCT of WPT system has been proposed in many papers to estimate the load resistance without feedback [Yang et al., 2018], to improve the efficiency with low costs [Tritschler et al., 2015] or by using a frequency-gap model, or to determine the switching frequency [Gao et al., 2017], but in this paper we proposed to improve the efficiency by changing the resonance frequency, optimizing the air gap, and fixing the Resistive load.

### 2.1 Basic analysis of WPT system

The IWPT transformer as shown in Figure 3 is characterized by a primary winding and secondary winding. The primary winding has both of a winding resistance  $R_1$ , and a self-inductance  $L_1$ . Similarly, the secondary winding has both of a winding resistance  $R_2$  and a self-inductance  $L_2$ . Due to the winding geometry and the conductor's proximity to the surface, parasitic capacitance appears between the turns of the windings and the layers; it thus becomes prominent at reliably high frequencies close to the self-resonance frequency of the transforming windings at high frequencies. This capacitance also called stray capacitance or self-capacitance of the winding. Parasitic capacitance was measured in three types of Litz wires in [Prasai and Odendaal, 2005]. It is assumed that the WPT transformer has an air core and the operating frequency is lower than the self-resonance frequency which leads to the neglect of the stray capacitance. A sinusoidal voltage source is used with an angular frequency  $\omega$ .

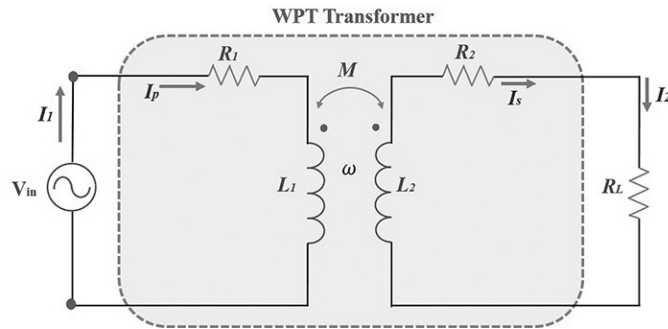


Fig. 3 Air core transformer representation

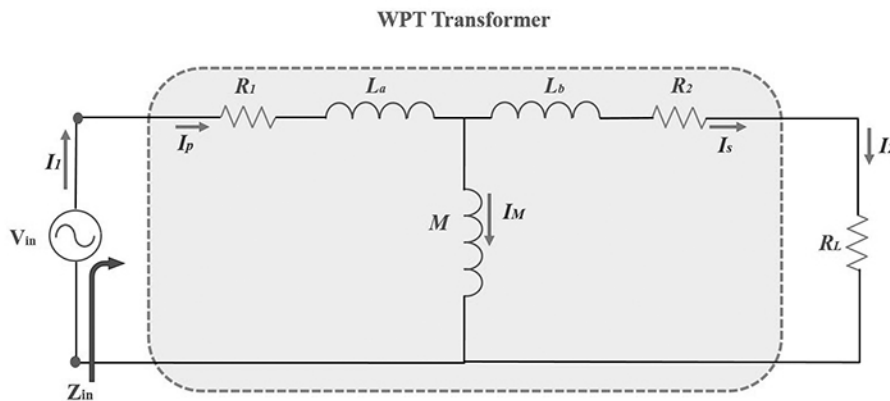


Fig. 4 The equivalent circuit of IWPT system

The resistive load  $R_L$  is occurred to receive the power transferred from the power source.

For comparable and easy analysis of the WPT circuit as in [Nilsson et al., 2015; Alexander and Sadiku, 2013], Figure 4 represents the equivalent circuit of inductive WPT system, where the leakage inductances of primary and secondary windings are  $L_a$  and  $L_b$  respectively; since  $L_a = L_1 - M$  and  $L_b = L_2 - M$ .

Figure 4 illustrates that the source and the load are directly connected to the resonator; which leads to solving the circuit simply by using Kirchhoff's Voltage Law (KVL) that get the following equations:

The KVL equation of the primary loop is:

$$V_{in} = (R_1 + j\omega(L_a + M)) I_1 - (j\omega M) I_2 \quad (1)$$

where the KVL equation of the secondary loop is:

$$0 = -(j\omega M) I_1 + [(R_2 + R_L) + j\omega(L_b + M)] I_2 \quad (2)$$

So, to find the total impedance  $Z_1$  which is the impedance of the network as seen by the source; Firstly, we Consider that:

$$Z_{11} = R_1 + j\omega(L_a + M) \quad (3)$$

$$Z_{22} = R_2 + R_L + j\omega(L_b + M) \quad (4)$$

By using coefficient matrix method, we get,

$$\begin{bmatrix} Z_{11} & -j\omega M \\ -j\omega M & Z_{22} \end{bmatrix} \begin{bmatrix} I_1 \\ I_2 \end{bmatrix} = \begin{bmatrix} V_{in} \\ 0 \end{bmatrix} \quad (5)$$

The impedance of the network as seen by the source when operating at an angular frequency  $\omega$  is given by

$$Z_{in} = R_1 + j\omega(L_a + M) + \frac{(\omega M)^2}{R_2 + R_L + j\omega(L_b + M)} \quad (6)$$

The real part of the input impedance of the network is

$$Z_{in,real} = R_1 + \frac{(\omega M)^2 (R_2 + R_L)}{(R_2 + R_L)^2 + (\omega[L_b + M])^2} \quad (7)$$

The imaginary part of the input impedance of the network is

$$Z_{in,img} = (\omega[L_a + M]) - \frac{(\omega M)^2 (\omega[L_b + M])}{(R_2 + R_L)^2 + (\omega[L_b + M])^2} \quad (8)$$

By definition that the efficiency of the transformer is defined as the ratio of useful power output to the input power which is denoted by

$$\eta = \frac{P_{out}}{P_{in}} = \frac{P_{out}}{P_{out} + P_{loss}} = \frac{R_L}{R_L + R_2 + R_1 \left( \left( \frac{R_2 + R_1}{\omega M} \right)^2 + \left( \frac{L_b + M}{M} \right)^2 \right)}$$

$$= \frac{R_L}{R_L + R_2 + \left( 1 + \frac{R_1(R_2 + R_1)}{\omega^2 M^2} \right) + R_1 \left( \frac{L_b + M}{M} \right)^2}$$
(9)

The efficiency of the transformer as a function of the coupling factor  $K = \frac{M}{\sqrt{L_1 L_2}}$  is

$$\eta = \frac{R_L}{R_L + R_2 + \left( 1 + \frac{R_1(R_2 + R_1)}{\omega^2 K^2 L_1 L_2} + \frac{R_1 L_2}{K^2 L_1} \right)}$$
(10)

The maximum efficiency of the power transfer can be satisfied if  $\omega \gg \sqrt{\frac{R_1(R_2 + R_1)}{K^2 L_1 L_2}}$  has occurred which in turns means that the term  $\frac{R_1(R_2 + R_1)}{\omega^2 K^2 L_1 L_2}$  should tend to zero.

So, the angular frequency in the system should be

$$\omega \gg \sqrt{\frac{R_1(R_2 + R_1)}{\omega^2 K^2 L_1 L_2}}$$
(11)

From this condition, the maximum theoretical efficiency is given

$$\eta_{max} = \frac{R_L}{R_L + R_2 + \frac{R_1 L_2}{K^2 L_1}}$$
(12)

The efficiency of the IWPT transformer model which is indicated in equation (10) relies on both of the system’s load, and primary and secondary windings of the IWPT transformer. It is clearly evident in the equation (11) that whenever the frequency has increased the efficiency of the system increases which in turn means that the frequency of the input voltage source should be reasonably high. To overcome the significant reduction in power factor resulting from the inductivity nature of the IWPT transformer model due to comparatively high frequencies and the impedance as seen by the source, which leads to large leak-

age inductances in both of the primary and secondary windings of the IWPT transformer. The decreasing of VA rating becomes necessary which will keep both the Power Factor (PF) and the efficiency as high as possible; to achieve this situation, the capacitive compensation in both primary and secondary windings is recommended to circumvent this problem.

### 2.2 Compensation analysis of IWPT System

Capacitive compensation has been applied in both the primary and secondary windings of the IWPT transformer for power factor correction and reactive power compensation, which turns to increase the efficiency of the IWPT transformer, increase the capability of the system, and correct the PF.

The main purpose of the capacitive compensation of primary winding of the IWPT transformer is decreasing the VA rating “the apparent power” that leads to increase the ratio of real power to apparent power until approaching unity, as the system becomes less reactive and more purely resistive, which turns to increase the system efficiency, however the secondary compensation is used to improve the power transfer capability of the IWPT transformer.

Depending on the connection method of the electronic parts in the electrical circuits, which are whether series or parallel, there are four basic topologies of capacitive compensations. These topologies are Series-Series (SS) capacitive compensation Topology, Series-Parallel (SP) capacitive compensation Topology, Parallel-Series (PS) capacitive compensation Topology, and Parallel-Parallel (PP) capacitive compensation Topology. In this paper, the SS capacitive

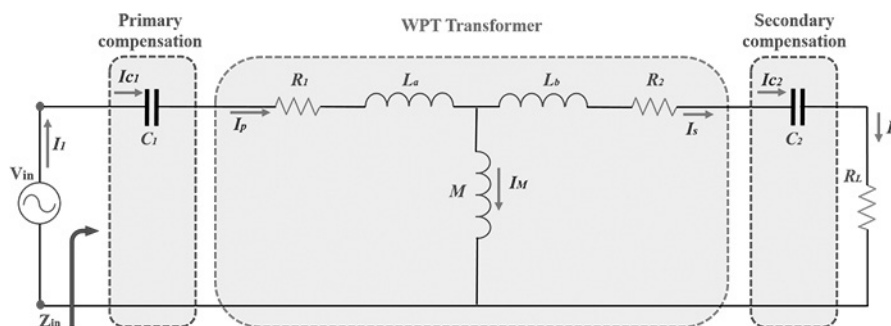


Fig. 5 The circuit diagram of SS topology representation

compensation Topology is discussed theoretically and experimentally. Figure 5 shows the circuit diagram of SS topology representation which used in this research to improve the IWPT transformer, where  $C_1$  and  $C_2$  are the primary and secondary capacitive compensations respectively.

By using KVL for solving the circuit, the KVL equation of the primary and secondary loops are given by equations (13) and (14) respectively as follow

$$V_{in} = \left( R_1 + j \left( \omega(L_a + M) - \frac{1}{\omega C_1} \right) \right) I_1 - (j\omega M) I_2 \quad (13)$$

$$0 = -(j\omega M) I_1 + \left( (R_2 + R_L) + j \left( \omega(L_b + M) - \frac{1}{\omega C_2} \right) \right) I_2 \quad (14)$$

To facilitate the process of finding the total impedance  $Z_{in}$  which is the impedance of the network as seen by the source, we considered that

$$Z_{11} = R_1 + j \left( \omega(L_a + M) - \frac{1}{\omega C_1} \right) \quad (15)$$

$$Z_{22} = R_2 + R_L + j \left( \omega(L_b + M) - \frac{1}{\omega C_2} \right) \quad (16)$$

Solving by using the coefficient matrix method, gives us,

$$\begin{bmatrix} Z_{11} & -j\omega M \\ -j\omega M & Z_{22} \end{bmatrix} \begin{bmatrix} I_1 \\ I_2 \end{bmatrix} = \begin{bmatrix} V_{in} \\ 0 \end{bmatrix} \quad (17)$$

Equation (17) can be solved by inverting the coefficient matrix to result the equation in terms of current

$$\begin{bmatrix} I_1 \\ I_2 \end{bmatrix} = \begin{bmatrix} Z_{11} & -j\omega M \\ -j\omega M & Z_{22} \end{bmatrix}^{-1} \begin{bmatrix} V_{in} \\ 0 \end{bmatrix} \quad (18)$$

The coefficient matrix in terms of current would be as follow

$$\begin{bmatrix} I_1 \\ I_2 \end{bmatrix} = \begin{bmatrix} \frac{Z_{22}}{Z_{11}Z_{22} + (\omega M)^2} & \frac{j\omega M}{Z_{11}Z_{22} + (\omega M)^2} \\ \frac{j\omega M}{Z_{11}Z_{22} + (\omega M)^2} & \frac{Z_{11}}{Z_{11}Z_{22} + (\omega M)^2} \end{bmatrix} \begin{bmatrix} V_{in} \\ 0 \end{bmatrix} \quad (19)$$

The impedance of the network as seen by the source when operating at an angular frequency  $\omega$  is given by

$$Z_{in} = R_1 + j \left( \omega(L_a + M) - \frac{1}{\omega C_1} \right) + \frac{(\omega M)^2}{R_2 + R_L + j \left( \omega(L_b + M) - \frac{1}{\omega C_2} \right)} \quad (20)$$

The real part of the input impedance of the network is

$$Z_{in-real} = R_1 + \frac{(\omega M)^2 (R_2 + R_L)}{(R_2 + R_L)^2 + \left( \omega(L_b + M) - \frac{1}{\omega C_2} \right)^2} \quad (21)$$

The imaginary part of the input impedance is

$$Z_{in-imag} = \left( \omega(L_a + M) - \frac{1}{\omega C_1} \right) - \frac{(\omega M)^2 \left( \omega(L_b + M) - \frac{1}{\omega C_2} \right)}{(R_2 + R_L)^2 + \left( \omega(L_b + M) - \frac{1}{\omega C_2} \right)^2} \quad (22)$$

Due to tuning the system, it is necessary to operate the IWPT system at secondary resonance frequency  $\omega_o$ . At this resonance frequency, the self-inductance of the secondary winding is fully compensated by the secondary capacitive compensation, and therefore, the impedance of the secondary winding as seen by the primary one is purely resistive in nature. Thus, the value of secondary capacitive compensation

$$C_2 = \frac{1}{\omega_o^2 (L_b + M)} = \frac{1}{\omega_o^2 L_2} \quad (23)$$

Since the power factor is important to be unity in any system to achieve high efficiency, which means that the frequency at which the system is required to resonate should be equal to the frequency at which the system actually resonates to achieve high power transfer capability between the primary and the secondary windings, which means both the operating frequency and the secondary resonance frequency will be commensurate. The secondary frequency is

$$\omega_o = \frac{1}{\sqrt{(L_b + M)C_2}} = \frac{1}{\sqrt{L_2 C_2}} \quad (24)$$

To improve the power factor to be unity, the imaginary part of the impedance at the operating frequency should be zero, so from equation (22) and equation (13) we get,

$$\left( \omega_o [L_a + M] - \frac{1}{\omega_o C_1} \right) = \frac{(\omega_o M)^2 \left( \omega_o [L_b + M] - \frac{1}{\omega_o C_2} \right)}{(R_2 + R_L)^2 + \left( \omega_o [L_b + M] - \frac{1}{\omega_o C_2} \right)^2} \quad (25)$$

Therefore, from equation (25), the primary capacitive compensation is devised as

$$C_1 = \frac{1}{\omega_o^2 [L_a + M] - \frac{(\omega_o M)^2 \left( \omega_o [L_b + M] - \frac{1}{\omega_o C_2} \right)}{(R_2 + R_L)^2 + \left( \omega_o [L_b + M] - \frac{1}{\omega_o C_2} \right)^2}} \quad (26)$$

$$C_1 = \frac{1}{\omega_o^2 L_1 - \frac{\omega_o^2 K^2 L_1 L_2 \left( \omega_o^2 L_2 - \frac{1}{C_2} \right)}{(R_2 + R_L)^2 + \left( \omega_o L_2 - \frac{1}{\omega_o C_2} \right)^2}}$$

In case  $|Z_{22}| \gg |jM|$ , both  $R_2$  and  $R_L$  can be neglected due to its small size. So, the primary capacitive compensation is devised as

$$C_1 = \frac{1}{\omega_o^2 [L_a + M] - \frac{(\omega_o M)^2}{\left( \omega_o [L_b + M] - \frac{1}{\omega_o C_2} \right)}} = \frac{1}{\omega_o^2 L_1 - \frac{\omega_o^2 K^2 L_1 L_2}{\left( \omega_o L_2 - \frac{1}{\omega_o C_2} \right)}} \quad (27)$$

But in case  $|Z_{22}| \ll |jM|$ ,

$\frac{(\omega_0 M)^2 \omega_0 [L_b + M] \frac{1}{\omega_0 C_2}}{(R_2 + R_L)^2 + \left(\omega_0 [L_b + M] - \frac{1}{\omega_0 C_2}\right)^2}$  can be neglected.

So, the primary capacitive compensation is devised as

$$C_1 = \frac{1}{\omega_0^2 (L_p + M)} = \frac{1}{\omega_0^2 L_1} \quad (28)$$

From both of equation (23) and equation (28), It is noted that the secondary capacitive compensation relies on the primary resonance frequency and the self-impedance of the secondary winding, if  $|Z_{22}|$  is so smaller than  $|jM|$ ; where the self-impedance of both the primary windings are just depending on their physical geometry.

By definition, the efficiency of the system  $\eta$  is defined as

$$\eta = \frac{P_{out}}{P_{out} + P_{loss}} = \frac{R_L}{R_L + R_2 + R_1 \left( \frac{R_2 + R_L}{\omega M} \right)^2}$$

By taking  $R_L + R_2$  as a common factor, we get

$$\eta = \frac{R_L}{(R_L + R_2) \left( 1 + \frac{R_1 (R_2 + R_L)}{\omega^2 M^2} \right)} \quad (29)$$

$$\eta = \frac{R_L}{(R_L + R_2) \left( 1 + \frac{R_1 (R_2 + R_L)}{\omega^2 K^2 L_1 L_2} \right)} \quad (30)$$

The maximum efficiency of the power transfer can be satisfied if  $\omega \gg \sqrt{\frac{R_1 (R_2 + R_L)}{K^2 L_1 L_2}}$  has occurred which in turns means that the term  $\frac{R_1 (R_2 + R_L)}{\omega^2 K^2 L_1 L_2}$  should tend to zero.

Therefore, the angular frequency in the system should be

$$\omega \gg \sqrt{\frac{R_1 (R_2 + R_L)}{K \sqrt{L_1 L_2}}} \quad (31)$$

From this condition, the maximum theoretical efficiency is given

$$\eta_{max} = \frac{R_L}{R_L + R_2} \quad (32)$$

From equation (32), we notice that the maximum efficiency does not depend on the resistance of the primary winding, but just relies on the resistive load and the resistance of the secondary winding.

### 3. EXPERIMENTAL RESULT

The (wf-1974) multifunction generator is used to generate the signals in the IWPT system. These signals are square waves and are changed from 10 kHz to 20 kHz. The output of this function generator is connected to the precision power amplifier 4520A which provide power to the IWPT system with 100 watts to

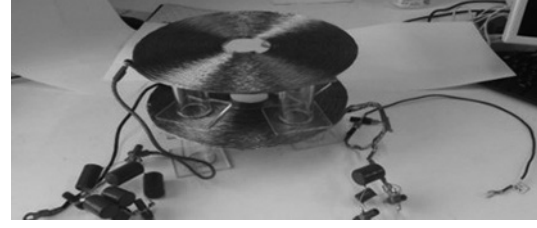


**Fig. 6** The experimental windings of the IWPT transformer

be transmitted wirelessly. Furthermore, two windings are made using Litz wires. The first winding is the transmitter winding, and the second one is the receiver winding. These coils used as an emitter and a receiver in the experimental setup are shown in Figure 6.

The configuration of the transmitter and receiver windings are shown in Figure 7.

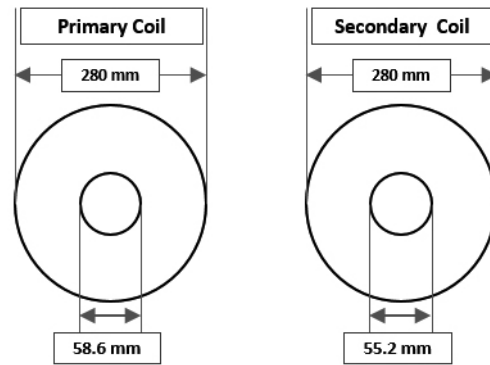


**Fig. 7** The configurations of the transmitter and receiver windings of the IWPT system

Table 1 shows out the configurations of the transmitter and receiver windings of the IWPT system.

**Table 1** The configuration's table of the transmitter and receiver windings of the IWPT system

Compressions	Primary coil	Secondary coil
Inner Diameter [mm]	58.6	55.2
Outer Diameter [mm]	280	280
Number of winding Turns [turns]	32	30
Self-Inductance [ $\mu$ H]	0.1645	0.13115
impedance of the windings $\Omega$	0.130523	0.5073665

#### 3.1 Analytical and practical implementation of WPT system

In section 2, analysis and design considerations for the SS compensated WPT topology are presented. Using these design criteria, analytical and practical implementation of a WPT system is presented in this section

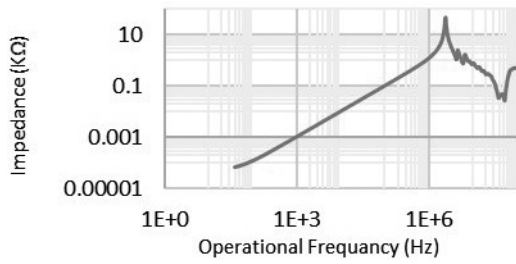


**Fig. 8** The behavior of the primary winding’s impedances with respect to the operating frequency

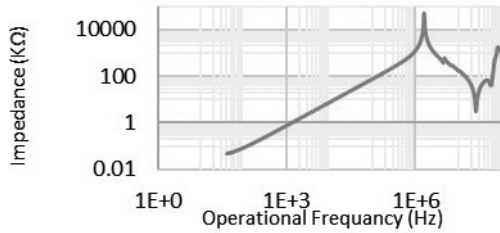


**Fig. 9** The behavior of the secondary winding’s impedances with respect to the operating frequency

since one of the major objectives of this experimental setup is to achieve high efficiency of the IWPT transformer with its compensation. Using Agilent 4294A precession impedance analyzer, the behavior of the winding’s impedances relying on the operating frequency are analyzed as shown in Figure 8 and Figure 9. The result shown in Figure 8 shows that the resistance of the primary winding is directly proportional to the frequency. The self-inductance of each winding is measured to adjust the parameters, and then the capacitive compensation is calculated for the resonance frequency of the operation frequency, the primary and secondary windings must be compensated with capacitors to achieve the resonance frequency at every operation frequency.

### 3.2 Experimental setup for the measurement of the frequency response at 10 kHz

Figure 9 shows the same result of Figure 8, since the relationship between the impedance of the winding and the operation frequency is a positive relationship until the frequency reaches about 5 MHz frequency. Figure 10 shows the characteristic impedance as a function of operating frequency which changes from 40 Hz to 100 MHz for both of the primary winding with its capacitive compensation and the secondary winding with its capacitive compensation. These figures show that the resonance frequency occurs at 10.053 kHz for both of the two windings. At this resonance frequency, 100 kHz, the primary and secondary windings must be compensated with capacitors of 0.8135  $\mu\text{F}$  and 0.812  $\mu\text{F}$  respectively. However,

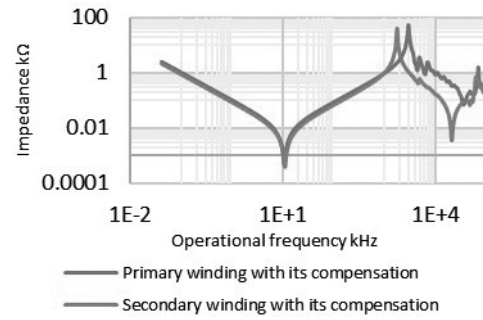


**Fig. 10** The characteristic impedance of the primary and the secondary windings with their series capacitive compensations resonating at 10 kHz

capacitors with these values are not available in the market. Therefore, combinations of parallel and series capacitors are used to obtain the values of the capacitive compensation; a 0.911  $\mu\text{F}$  and 0.913  $\mu\text{F}$  capacitors are used for primary and secondary compensation respectively.

After placing the windings on top of each other in parallel and connecting the primary winding with the 100-Watt AC power source, and connecting the secondary winding with the load, both the input and output parameters are measured to find the efficiency. Figure 11 shows the comparison between the efficiency of 50 mm and 100 mm distances at the operational frequency varying from 9.5 kHz to 10.9 kHz. This figure shows that the power transfer reaches the maximum point at 10.493 kHz when the distance between the windings is 50 mm, but it reaches maximum power transfer at 10.7 kHz when the distance is 100 mm. This result is due to the reduction of the mutual inductance between the winding at large air gaps between the primary and secondary windings.

After setting the experiments of transferring power at frequency 10 kHz, the efficiencies of the transformer are measured at distances of 50 mm and 100 mm and the compression between them is put in Figure 11.

At the same capacitive compensations which are  $C_1 = 0.81 \mu\text{F}$ , and  $C_2 = 0.91 \mu\text{F}$ , we noted that the efficiency

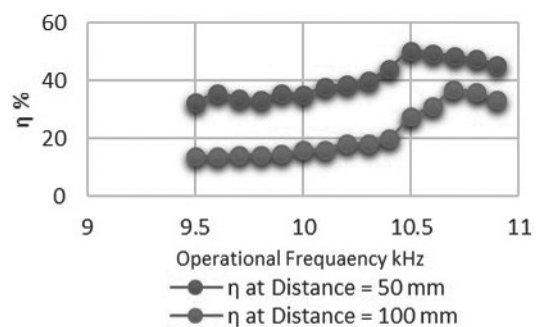


**Fig. 11** Measured efficiency for frequency at 10 kHz for distances of 50 mm and 100 mm

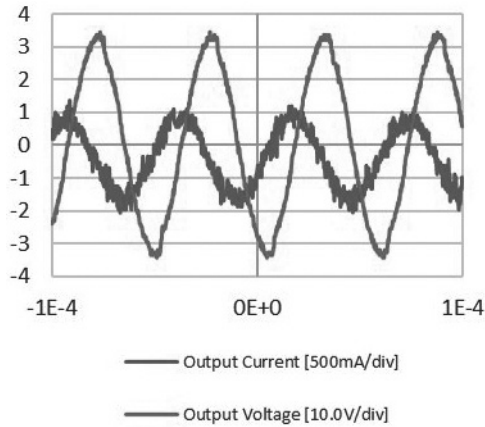


**Fig. 12** The secondary's currents and voltage outputs at 10 kHz

at distance 50 mm is higher and reaches its peak at resonance frequency 10.65 kHz. There is a difference in the resonance because of the effect of Mutual inductance between windings.

### 3.3 Experimental setup for the measurement of the frequency response from 11 to 20 kHz

The same procedures of the first experiment of transferring power at 10 kHz operating frequency are used in the experiments of transferring power at operating frequencies varying from 11 to 20 kHz. Results are shown in Figures 13-18.

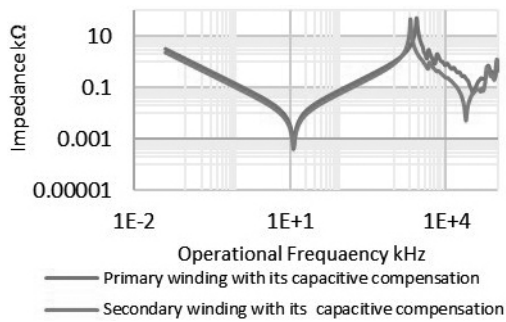


**Fig. 13** The characteristic impedance of the primary and secondary windings resonating at 11 kHz

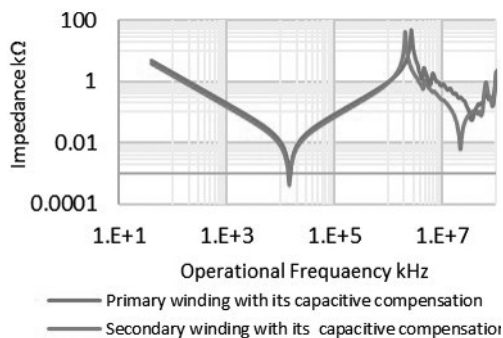


**Fig. 14** The characteristic impedance of the primary and secondary windings resonating at 12 kHz

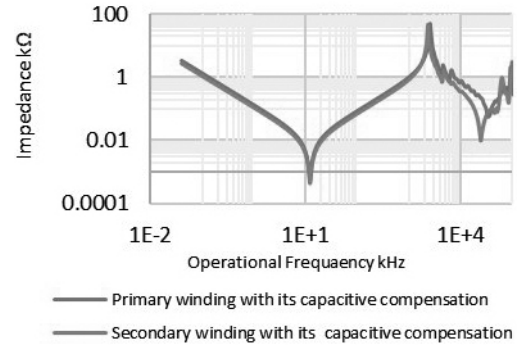


**Fig. 15** The characteristic impedance of the primary and secondary windings resonating at 12 kHz

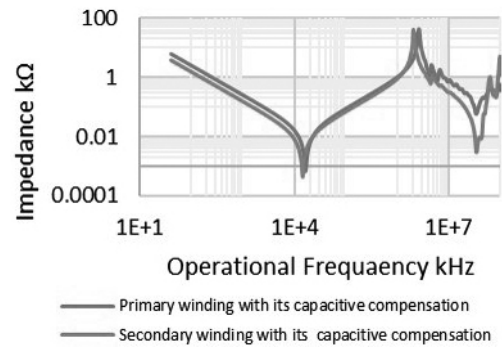


**Fig. 16** The characteristic impedance of the primary and secondary windings resonating at 16 kHz

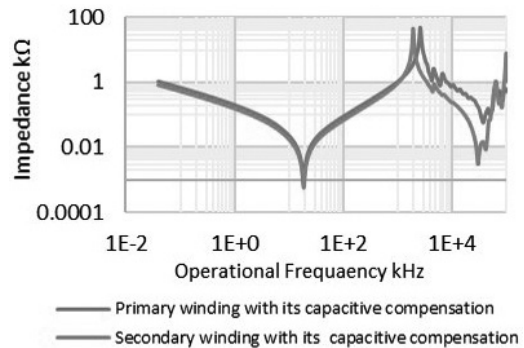


**Fig. 17** The characteristic impedance of the primary and secondary windings resonating at 18 kHz

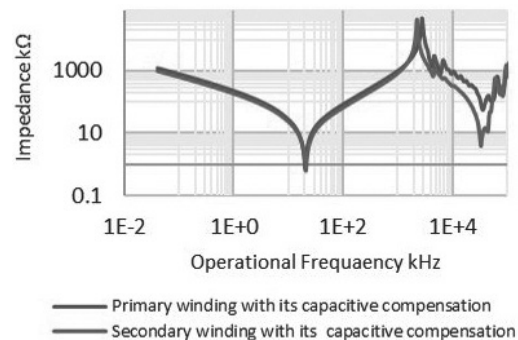


**Fig. 18** The characteristic impedance of the primary and secondary windings resonating at 20 kHz

At low frequencies, the capacitive reactance is high; which means that the capacitive reactance is much larger than the impedance of the winding at low frequencies, so most power is absorbed by the capacitor. As the frequency increases, the capacitive reactance decreases until it becomes equivalent to the inductive reactance of the winding at a specific frequency (the resonance frequency). Figure 13 to Figure 18 show that both the behavior of the characteristic impedances of both of the primary and secondary windings are the same at low frequencies, but the behavior becomes more unstable at high frequencies. This implies that another resonance frequency appears at the high frequencies. The efficiency at this resonance frequency is lower than the efficiency of the adjusted resonance frequency. On the other hand, the phase angle of the characteristic impedances of both of the primary and secondary windings are not the same due to many factors such as the vibration of the connectors of the windings, where the low capacitance and inductance should be taken into account because of its significant impact on the behavior of the characteristic impedances of windings at high frequencies. This vibration

caused by high frequency is neglected in this research because the system operates at 10-20 kHz frequency range. There are differences between the calculated values of the desired capacitive compensation and the experimental capacitors used in the test, which led to a lack of efficiency. Its effect on the resonance can be shown clearly in Figure 19. This slight difference in capacitive compensations can change the efficiency due to its significant impact on resonance frequency. The primary winding resonates at 10.2 kHz while the secondary resonates at 10.7 kHz.

The WPT transformer parameters have to be well defined to make a comparison based on the achievable efficiency of transferred power, so the measured WPT transformer parameters are tabulated in Table 2.

The After setting up the experiments to measure the efficiency of the WPT transformer at different resonance frequencies between 11-20 kHz; the efficiencies are as follows:

Figure 20 and Figure 21 show the efficiency of the WPT transformers at resonance frequencies 11 kHz and 12 kHz respectively. the efficiencies of these resonance frequencies which operate in 9.5-13 kHz

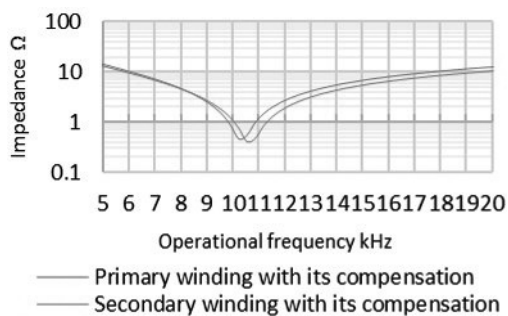


Fig. 19 The characteristic impedance of the primary and secondary windings resonating at 10 kHz

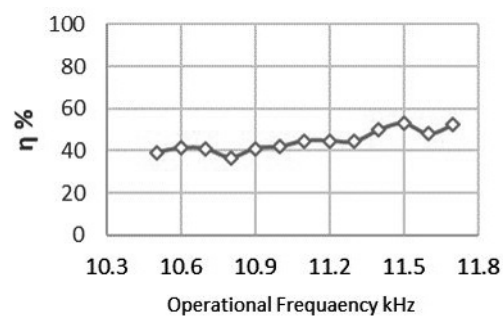
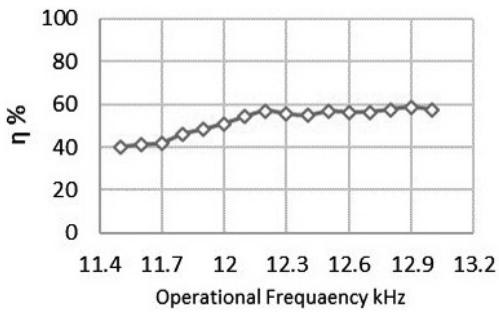


Fig. 20 Measured efficiency  $\omega_0$  at 11 kHz for distances 50 mm

Table 2 The WPT transformer parameters

Frequency kHz	Calculated Capacitance (CAL) $\mu\text{F}$		Experimental Capacitance (EXP) $\mu\text{F}$		$\Delta C = \text{CAL} - \text{EXP}$		Measured Inductance	
	primary	secondary	primary	secondary	$\Delta C_1 \mu\text{F}$	$\Delta C_2 \mu\text{F}$	$L_1 \text{ mH}$	$L_2 \text{ mH}$
10	0.8135	0.9110	0.812	0.913	1.4E-03	-1.9E-03	0.1645	0.13115
11	0.6723	0.7529	0.6722	0.7528	9.8E-05	1.4E-04	0.1645	0.13115
12	0.5649	0.6327	0.56492	0.6325	-2. E-06	1.97E04	0.1645	0.13115
13	0.4813	0.5391	0.4812	0.538	1.5E-05	10.8E-04	0.1645	0.13115
14	0.4150	0.4648	0.415	0.4648	4.1E-05	2.5E-05	0.1645	0.13115
15	0.3615	0.4049	0.3615	0.4048	4.7E-02	1.1 E-04	0.1645	0.13115
16	0.3178	0.3559	0.315	0.3558	2.7E-02	6.2E-05	0.1645	0.13115
17	0.2815	0.3153	0.2815	0.315	-1.8E-05	2.4E-04	0.1645	0.13115
18	0.2511	0.2812	251	0.2824	7.4E-05	-1.2E-03	0.1645	0.13115
19	0.2253	0.2524	0.225	0.2522	3.4E-04	1.7E-04	0.1645	0.13115
20	0.2034	0.2278	0.2033	0.22775	7.0E-05	1.4E-05	0.1645	0.13115



**Fig. 21** Measured efficiency for resonance frequency at 12 kHz for distances 50 mm

operational frequency ranges did not exceed 70 %, but it is clearly noted that the efficiency is directly proportional to the frequency at the same conditions. The efficiencies of the higher frequencies experiments are also done and the results are shown in Figures 22-25. Figure 26 shows the efficiency for all experiments as a function of the resonance frequency. It can be noted that the efficiency is up to 80 %

The output is connected to a fixed resistive load which is five ohms, the power transferred through the transformer is 100 Watt and should be achieved to this

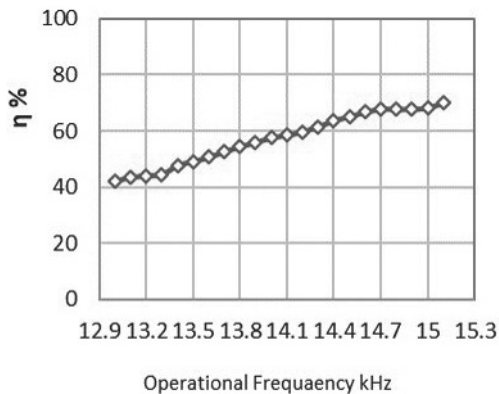


**Fig. 22** Measured efficiency for resonance frequency at 14 kHz for distances 50 mm

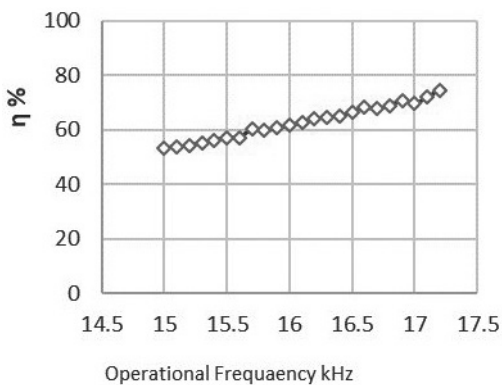


**Fig. 23** Measured efficiency for resonance frequency at 16 kHz for Distances 50 mm

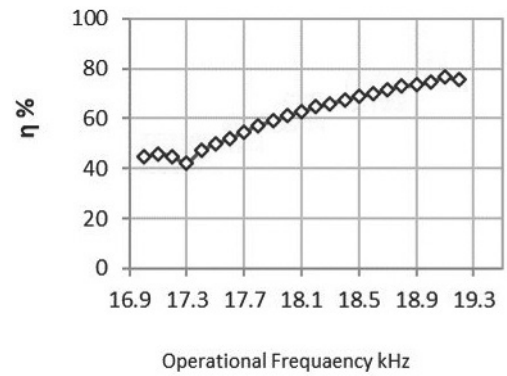


**Fig. 24** Measured efficiency for resonance frequency at 18 kHz for distances 50 mm

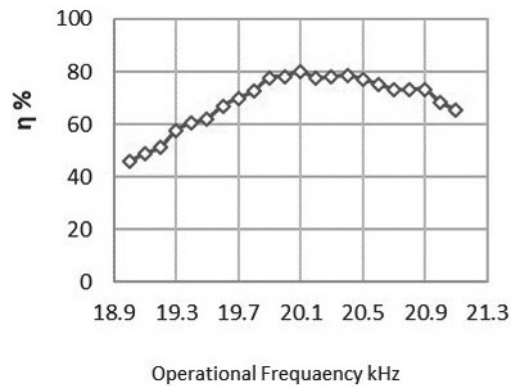


**Fig. 25** Measured efficiency for resonance frequency at 20 kHz for distances 50 mm

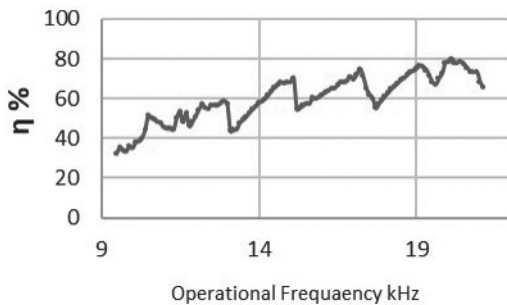


**Fig. 26** The efficiency as a function of the resonance frequency for all the experiments

load.

To compare the analytical result which is given by Equation (30) with the experimental set-up, Figure 27 focuses on the frequencies ranges from 10-20 kHz for both the analytical result with the experimental results.

It can be noted that in Figure 27 there is a difference in the efficiency by 10 % due to the neglected eddy current losses and the skin effect. In addition to the previous reasons, there is a difference in the desired capacitive compensation values and the available capacitors used in the laboratory. At high frequencies,

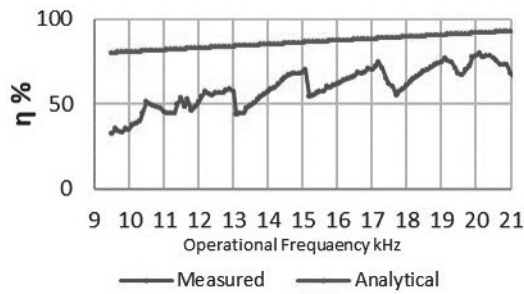


**Fig. 27** The analytical efficiency as a function of the resonance frequency for all the experiments

there are differences in the efficiency less than the differences at low frequencies because of the changing of the of the Impedance which was neglected from equation (26). The fluctuation in the chart could be explained by the effect of the difference between the capacitor values used in the experiments and the original calculated values; this simple difference has a significant impact which causes these fluctuation and reduces the efficiency.

The same steps have been done for the loads 1  $\Omega$ , 3  $\Omega$ , and 7  $\Omega$  to compare them with 5  $\Omega$  load as shown in Figure 28.

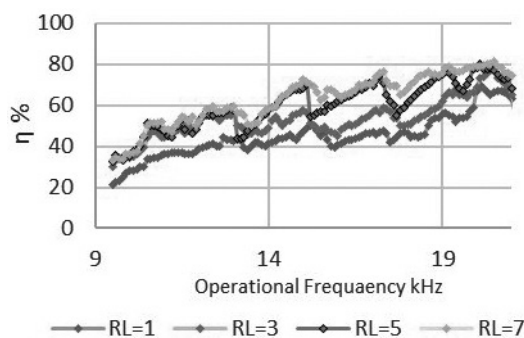


**Fig. 28** The comparison among measured efficiencies for different loads

From Figure 28, It was noted that the efficiency is directly proportional to the load resistance value, but at 19 kHz and 20 kHz the efficiencies of both 5  $\Omega$  and 7  $\Omega$  approximately the same, which allows us to make 5  $\Omega$  as a load's case study in this paper.

#### 4. CONCLUSION

This research aims to design and optimize a wireless power transfer link for electric vehicles "Disabled scooter or Electric bikes". The method of the short-range resonance inductive coupling has been employed and discussed analytically and experimentally for achieving this goal, and the wireless power transfer with its capacitive compensation was discussed

analytically.

The series-series capacitive compensation method has been reviewed to justify the need for a fully optimized short-range resonance inductive coupled system, that is capable of wirelessly transferring adequate power to small-size electric vehicles. Specific modeling terms and analytical design for a full definition of the transformers of the WPT system have been introduced and described with equations, with emphasis on the use of Litz wire. Also, the power transfer efficiency of the system has been analyzed. On the other side, a power transfer circuit which is a function generator with a power amplifier is used, and designed transformer parameters and specifications have been described. Relationships for input and output power with other electrical parameters have been defined to simplify the process of maximizing the power transferred by the WPT transformer. The power transferred in this system was 100 watt with a constant voltage of 20 volts. Finally, a complete analytical description with its exponential implementation to optimize the maximum efficiency of the WPT system has been developed. The design and optimization process have been implemented to create a coupling system, namely Short-Range Inductive Coupling with SS capacitive compensation that operates in the 10-20 kHz frequency ranges. The efficiency achieved for the systems is 80 % at a coil distance of 50 mm with resonance frequency matching the 20 kHz.

#### References

- Alexander, C. K. and Sadiku, M. n. o., *Fundamentals of electric circuits*, 5th ed., McGraw-Hill, 2013.
- Bibirica, C., Cristian, S., Ene, L., and Iordache, M., Improving the performance of PCB inductors for WPT systems using magnetic shields, *The 5th International Symposium on Electrical and Electronics Engineering*, 1-5, 2017.
- Choi, B. G., Sohn, Y. H., Lee, E. S., Han, S. H., Kim, H. R., and Rim, C. T., Coreless transmitting coils with conductive magnetic shield for wide-range ubiquitous IPT, *IEEE Transactions on Power Electronics*, 1-1, 2018.
- Chopra, S. and Bauer, P., Analysis and design considerations for a contactless power transfer system, *IEEE 33rd International Telecommunications Energy Conference*, 1-6, 2011.
- De-Boeij, J., Lomonova, E., and Vandenput, A., Contactless energy transfer to a moving load Part I: Topology synthesis and FEM simulation, *IEEE International Symposium on Industrial Electronics*, Vol. 2, 739-744, 2006.
- Fernández, C., García, O., Prieto, R., Cobos, J. A., Gabriels, S., and Borgh, G. V. D., Design issues of a

- core-less transformer for a contact-less application, *APEC, Seventeenth Annual IEEE Applied Power Electronics Conference*, Vol. 1, 339-345, 2002.
- Gao, Y., Tse, Z. T. H., and Ginart, A., Analytical method for mutual inductance and optimum frequency calculation in a series-series compensated inductive power transfer system, *IEEE Applied Power Electronics Conference and Exposition*, 3720-3722, 2017.
- Hassan, M. A. and Elzawawi, A., Wireless power transfer through inductive, *Institute for Natural Sciences and Engineering INASE*, Vol. Recent advances in circuits, 115-118, 2015.
- Honjo, T., Koyama, T., Umetani, K., and Hiraki, A. E., Novel receiving coil structure for improving efficiency and power transfer capability of resonant inductive coupling wireless power transfer, *19th International Conference of Electrical Machines and Systems*, 1-6, 2016.
- Huang, L., Hu, P., Swain A., A resonant compensation method for improving the performance of capacitively coupled power transfer system, *IEEE Energy Conversion Congress and Exposition*, 870-875, 2014.
- Nilsson, J. W. and Riedel, S. A., *Electric circuits*, Tenth ed., 729-731, PEARSON, 2015.
- Prasai, A. and Odendaal, W., Utilizing stray capacitances of a litz wire, *Fourtieth IAS Annual Meeting. Conference Record of the 2005 Industry Applications Conference*, Vol. 3, 1876-1883, 2005.
- Ramezani, A., Farhangi, S., Iman-Eini, H., and Farhangi, B., High efficiency wireless power transfer system design for circular magnetic structures, *IEEE Power Electronics and Drive Systems Technologies Conference*, 565-570, 2016.
- Shen, L., Tang, W., and Xiang, H., Uniform magnetic field of the planar coil with new winding structure for displacement-insensitive WPT, *IEEE International Conference on Communication Problem-solving*, 394-396, 2014.
- Tritschler, J., Goeldi, B., Reichert, S., and Griepentrog, G., Comparison of different control strategies for series-series compensated inductive power transmission systems, *17th European Conference on Power Electronics and Applications*, 1-8, 2015.
- Yang, Y., Jiang, Y., Tan, S-C, Hui, S-Y R., A frequency-sweep based load monitoring method for weakly-coupled series-series compensated wireless power transfer systems, *IEEE PELS Workshop on Emerging Technologies: Wireless Power Transfer*, 1-5, 2018.

(Received November 30, 2018; accepted December 27, 2018)